Chiang Mai J. Sci. 2013; 40(1) : 99-108
http://it.science.cmu.ac.th/ejournal/
Contributed Paper

Synthesis and Room Temperature Magnetic Behavior of Nickel Oxide Nanocrystallites

Kwanruthai Wongsaprom*[a] and Santi Maensiri [b]

[a] Department of Physics, Faculty of Science, Mahasarakham University, Mahasarakham, 44150, Thailand.

[b] School of Physics, Institute of Science, Suranaree University of Technology, Nakhon Ratchasima, 30000, Thailand.

*Author for correspondence; e-mail: wkwanruthai@gmail.com

Received: 28 November 2011
Accepted: 29 June 2012

ABSTRACT

Nickel oxide (NiO) nanocrystallites with a crystal size of around 54 nm have been synthesized via the polymerized complex method. The synthesized precursor was calcined at 873 K for 4 h to obtain the nickel oxide nanocrystallites. The XRD and electron diffraction analysis results indicated that the calcined sample has a cubic structure without any impurity phases. The FT-IR analysis result confirmed the formation of NiO. The NiO nanocrystallites exhibited UV absorption below 2.76 eV and the estimated direct band gap (E_g) of 3.06 eV. The Room temperature magnetization result revealed a ferromagnetic-like behavior and a coercivity of 149 Oe. The ferromagnetic-like properties are attributed to the lattice distortion and broken bond in the NiO nanocrystallites.

Keywords: nickel oxide, nanocrystallites, magnetic behavior, cubic structure, polymerized complex (PC) method

1. INTRODUCTION

Magnetism of nanoscale oxide particles with crystal sizes of less than 100 nm has generated increasing interest due to their unique magnetic properties; which significantly differ from those observed for their microcrystalline counterparts [1-3]. Antiferromagnetic nanoparticles have recently gained increased attention by virtue of their potential for exhibiting magnetization reversal by quantum tunneling [4-5]. Finite size effect induces anomalous magnetic behavior, which differs markedly from that found in the corresponding bulk material. This effect leads to an increase in the (i) fraction of atoms present on or near the surface and (ii) number of defect and missing bonds. Consequently, the coordination number is reduced which, in turn, causes a modification in the exchange interaction between the surface atoms [6]. The ultra-fine particles of transition metal oxides (eg. CoO, MnO and NiO) have been investigated by several research groups due to their abnormal magnetic behavior, small size and surface effects [7-9]. Moreover, when the sizes of the particles are reduced, the fraction of the total number with uncompensated spins will increase greatly [10]. Kodama et al.

[11] reported that the moments in antiferromagnetic nanoparticles of NiO are too large to be explained by a two-sublattice model. Numerical modeling of spin configurations included two, four, six and eight-sublattice configurations, indicating that a finite size effect, in which the reduced coordination of surface spins causes a fundamental change in the magnetic order throughout the particle sizes [12-13]. In 1991, Richardson *et al*. [13] reported that the presence of higher oxidation state centers, such as Ni^{3+} nickel oxide nanoparticles, did not contribute significantly to the particle magnetic moment responsible for superparamagnetic behavior. The measured magnetic susceptibility of nickel oxide particles was inversely proportional to the particle size for nickel oxide nanoparticles prepared by the thermal decomposition method. Ichiyanangi *et al*. [14] observed the presence of superparamagnetic or ferromagnetic behaviors of NiO nanoparticles with particle size in the 2-6 nm range by annealing $Ni(OH)_2$ monolayer-nanoclusters at a temperature above 973 K, in air. These samples showed ferromagnetic behavior with narrow hysteresis loops and coercivityof about 750 Oe at 5 K. The superparamagnetic behavior was observed between the temperature of 30 and 100 K. These behaviors should be due to the uncompensated surface spin, particularly for extremely small particles. Bi *et al*. [15] reported the ferromagnetic-like behavior of NiO nanoparticles with a grain size of 5 nm synthesized by the vacuum thermolysis method. The authors suggested that the large net magnetization was attributed to the reduced coordination and broken bonds combined with lattice distortion. However, the intrinsic origin of superparamagnetic and ferromagnetic behaviors in NiO fine particles has never been completely explained.

It is obvious that despite several reports and a lot of observations, inconsistency continuous to persist with regard to the behavior of NiO nanoparticles. Further, a literature survey suggests that the characteristics of NiO depend on the crystal size and distribution in addition to the synthesis route and experimental conditions. In this paper, we report the synthesis and magnetic properties of NiO nanocrystalline powders by a polymerized complex (PC) method [16]. The simple method has been successfully used by our group to synthesize $La_{0.5}Sr_{0.5}Co_{0.015}Ti_{0.985}O_{3-\delta}$ and $La_{0.5}Sr_{0.5}Fe_{0.015}Ti_{0.985}O_{3-\delta}$ diluted magnetic oxide nanoparticles with particle sizes of ~ 12-14 nm [17-18], Co-doped ZnO diluted magnetic oxide nanoparticles with particle sizes of ~ 38-55 nm [19] and nanocrystalline hydroxyapatite powders with particle sizes of ~ 16-125 nm [20]. The synthesized precursor was calcined at 873 K for 4 h to obtain the NiO nanocrystalline powders. The synthesized powders were characterized by X-ray diffraction (XRD), scanning electron microscopy (SEM), transmission electron microscopy (TEM), ultraviolet-visible spectroscopy (UV-Vis) and Fourier transform infrared spectroscopy (FT-IR). The magnetic properties of NiO powders were investigated using a superconducting quantum interference magnetometer (SQUID) at room temperature.

2. MATERIAL AND METHODS

In this study, nickel (II) nitrate hexahydrate (Aldrich, ≥ 99.999%), citric acid (BDH Laboratory Supplies, 99.7%) and ethylene glycol (Carlo Erba Reacgenti, 99.5%) were used as the starting chemicals. In a

typical procedure, 23.3489 g of citric acid was first dissolved in 25 ml ethylene glycol under vigorous stirring at 353 K. Subsequently, 3.2312 g of nickel nitrate hexahydrate was slowly added to this solution. Then, the solution was stirred at 423 K until the formation of the dark green colored polymer, between ethylene glycol and metal citrate complexes, was promoted. The highly viscous polymeric product obtained was then decomposed to a dark mass precursor, for several hours in air, until dry. Throughout the whole process described above, no pH adjustment was made. Finally, the dried precursor was calcined in a box-furnace at 873 K for 4 h in air. The calcined sample was ground to break up large agglomerates. The final product obtained was a dark green NiO nanocrystalline powder.

The prepared NiO sample was characterized by XRD at room temperature using a Philips X-ray diffractometer (PW3040), working with CuKa radiation in the 2θ range of 30°-90°. FT-IR spectra of the powders (as pellets in KBr) were recorded using a Fourier transform infrared spectrometer (Spectrum One FT-IR spectrometer, PerkinElmer Instrument, USA) in the range of 4,000-400 cm^{-1} with a resolution of 1 cm^{-1}. The morphology of the prepared sample was identified by SEM (LEO SEM 1450VP, UK), and TEM (Hitachi H8100 200kV conventional). The sample for TEM analysis was deposited on holey carbon film that was supported by a copper grid. The optical absorption spectra were measured in the range of 200-800 nm using a UV-3101PC UV-VIS-NIR scanning spectrometer (Shimadzu, Japan). The magnetic properties of the calcined powder were examined at room temperature (300K) using a SQUID magnetometer.

3. RESULTS AND DISCUSSION

The structure of the NiO sample was primary examined by XRD. The XRD pattern of the calcined NiO sample is shown in Figure 1(a). The calcined sample exhibits peaks that correspond to the (111), (200), (220), (311) and (222) planes for cubic structure of NiO as in standard data (JCPDS: 78-0429). The cubic lattice parameter *a* calculated from the XRD spectra for NiO powders is 0.4175±0.0001 nm and is close to the lattice constant, a = 0.4177 nm, from standard data (JCPDS: 78-0429). From the line broadening of corresponding X-ray diffraction peaks, the crystallite sizes (*D*) were estimated using the Scherrer and Williamson-Hall equations [21-22].

In the Scherrer equation

$$D = \frac{0.89\lambda}{\beta\cos\theta} \quad (1)$$

where λ is the wavelength of the X-ray radiation, *K* is a constant taken as 0.89, θ is the diffraction angle, and β is the full width at half maximum (*FWHM*).

Williamson-Hall's approach separates the effects of size and strain in the sample, using the equation:

$$\beta_{total} = \beta_{size} + \beta_{strain} = \frac{0.9\lambda}{D\cos\theta} + \frac{4.(\Delta d)\sin\theta}{d\cos\theta} \quad (2)$$

where β_{total} is the full width at half maximum of the XRD peak, λ is the incident X-ray wave length, θ is the diffraction angle, *D* is the crystal size and Δd is the difference of the *d* spacing corresponding to a typical peak. A plot of $\beta_{total}\cos\theta$ against $4\sin\theta$ yields the crystal size from the intercept value and the strain $\left(\frac{\Delta d}{d}\right)$ from the slope. The Williamson-Hall plots for the nickel oxide sample are shown in Figure 1(b). The line broadening can be used to obtain information about the

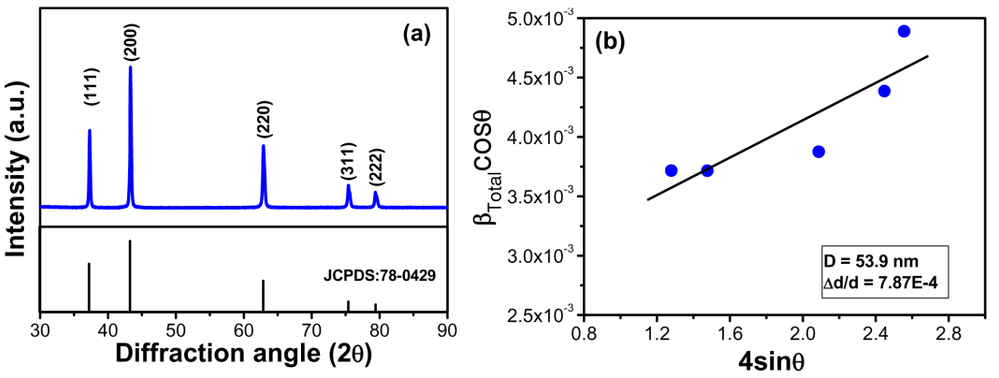

Figure 1. (a) XRD pattern and (b) the linear fitting using Williamson-Hall relationship of NiO nanocrystallites calcined in air at 873 K for 4 h.

crystal sizes of the nickel oxide sample, and the Scherrer and Williamson-Hall equations have been used for this purpose. The crystal sizes obtained from the sample, as calculated by Scherrer and Williamson-Hall equations, were 31.3 ± 3 nm and 53.9 ± 2 nm, respectively. The crystal sizes as determined by using the Williamson-Hall equation were larger than those calculated with the Scherrer equation, since this one does not take into account the effect of the lattice defects in the line broadening. From the Williamson-Hall plot, a lattice distortion ratio (strain) of (7.87 ± 2.48) × 10^{-4} is obtained, indicating a large lattice distortion in the nickel oxide nanocrystallites. The crystal sizes of NiO are shown in table 1, which also includes the crystal size of NiO nanocrystalline powders as calculated from the Scherrer formula as reported by Thota and Kumar [6] and Qiao et al. [23] for comparison. It can be seen that the crystal sizes were larger than those reported by Thota and Kumar [6] and Qiao et al. [23]. Different conditions and different synthesis routes may result in the range of crystal sizes of NiO.

The formation of a NiO bond was supported by FT-IR spectra as shown in Figure 2. In the FT-IR spectra, main bands were observed at ~3400, 2900, 1600, 1400, 1021 and 430 cm^{-1}. The band at ~3400 cm^{-1}

Table 1. Crystal sizes of NiO nanocrystalline powders synthesized by different methods.

NiO nanocrystalline powders	Crystal size determined from Scherrer formula (nm)	crystal size estimated from TEM studies (nm)	Crystal size determined from Williamson-Hall equation (nm)
PC method	31.3 ± 3	< 55	53.9 ± 2
Sol-gel method (Thota and Kumar, [6])	22	-	–
Anodic arc plasma method (Qiao et al., [23])	23	25 -	-

represented stretching of the O-H group. The band at ~2900 cm^{-1} was due to the C-H bond of the organic compounds. Two small peaks at ~1600 and 1400 cm^{-1} can be attributed to the asymmetric and symmetric stretching vibrations of coordinated carboxylate groups [19,24]. A small band at ~1,021 cm^{-1} was observed and can be assigned to the deformation vibration of C=O [25-26]. The strong peak at ~430 cm^{-1} was assigned to banding vibration of NiO [24].

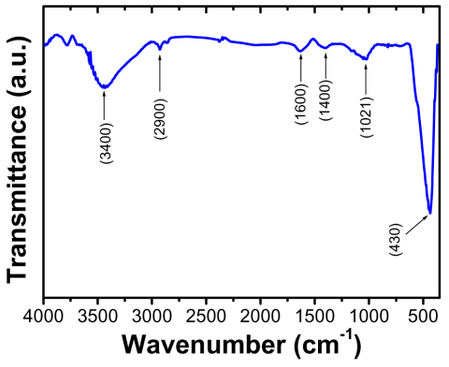

Figure 2. FT-IR spectra of the NiO nanocrystallites calcined in air at 873 K for 4 h.

The morphology of the NiO sample was studied by SEM. The SEM micrograph shows agglomerated particles as depicted in Figure 3(a). The agglomeration could be induced by densification resulting from the narrow space between particles due to the uniform distribution of oxidized metal anions in the three-dimensional polymeric network structure [27]. The nanocrystallites tend to agglomerate during synthesis or delivery process due to their high surface area and surface energy. The morphology and structure of the nanocrystallites calcined at 873 K were further revealed by TEM. TEM bright field image with corresponding selected-area electron diffraction patterns (SAED) of the NiO sample is shown in Figure 3(b). The nanocrystallites are smaller than 55 nm in size. The particle size of the NiO sample estimated from TEM bright field image is consistent with the result obtained using the Williamson-Hall equation. The SAED patterns (inset in Figure 3(b))

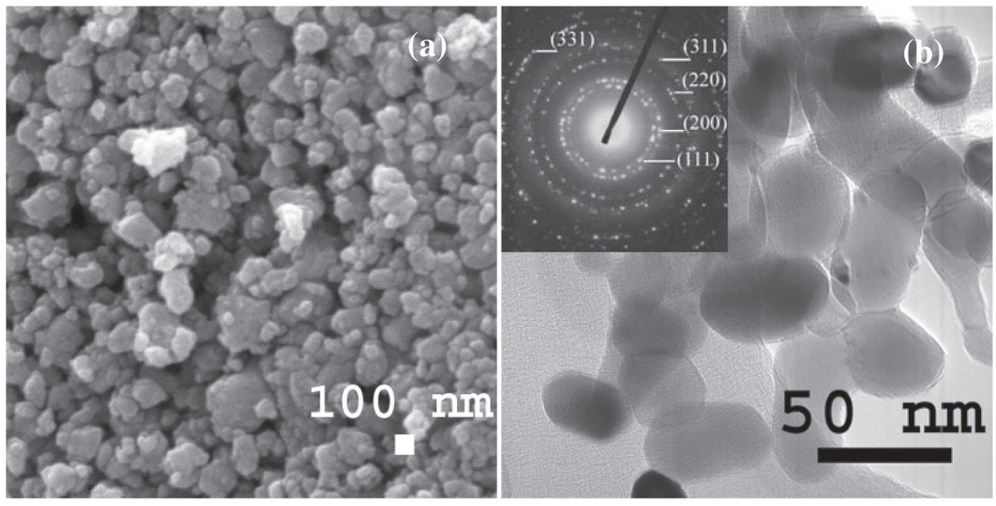

Figure 3. Electron microscopy images of nanocrystalline NiO powders calcined at 873 K: (a) SEM secondary electron image; (b) TEM bright field image with SAED patterns (inset).

of the NiO sample calcined at 873 K show spotty ring patterns without any additional diffraction spots and rings of Ni and other phases, revealing their cubic structure which is in agreement with the XRD result and standard data (JCPDS: 78-0429). According to the diffraction patterns in the insets of Figure 3(b), lattice constants measured agree with those of (111), (200), (220), (311) and (331) planes in standard data (JCPDS: 78-0429).

The UV-visible absorption spectrum of the NiO sample is shown in Figure 4. The sample shows a strong absorption below 450 nm (2.76 eV) with a well-defined absorbance peak at around 300 nm (4.13 eV). The band gap can be determined by fitting the absorption data to the direct transmission equation by extrapolating of the linear portions of the curves to absorption equals zero (inset of Figure 4).

$$\alpha h\nu = E_D(h\nu - E_g)^{1/2}, \qquad (3)$$

where α is the optical absorption coefficient, $h\nu$ is the photon energy, E_g is the direct band gap, and E_D is a constant [28]. The estimated band gap of the NiO is obtained to be 3.06 eV. This value is lower than the band gaps that are reported from thin films and bulks of NiO (3.2-4.0 eV) [29-31]. The difference in the band gap values which range from 3.0 to 4.0 eV is one of the curious features of the literature on NiO. Uplane et al. [29] reported three different E_g values of 3.3, 3.35 and 3.4 eV for NiO thin films and found that they decreased when the annealing temperature increased. They suggested that the higher temperature may improve the crystallinity of NiO which slightly changed the refractive index. These phenomena have been also observed in ZnO nanoparticles reported by Maensiri et al. [32].

Figure 5 shows the field dependence of the specific magnetization (M-H curve) of NiO nanocrystalline powders measured at 300 K. The calcined NiO sample exhibits ferromagnetic-like behavior after subtracting the diamagnetic contribution from the gel cap sample holder. The M-H curve of the NiO sample indicates hysteresis

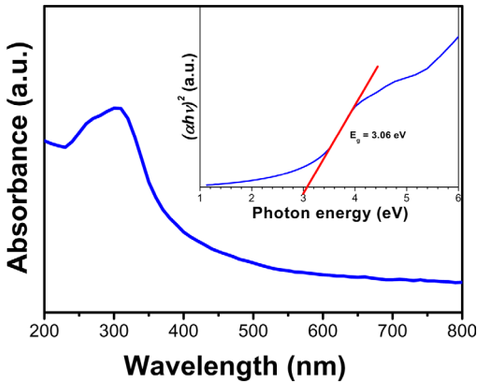

Figure 4. Room temperature optical absorbance spectrum of the NiO sample calcined 873 K. The inset shows plot of $(\alpha h\nu)^2$ as a function of photon energy for the NiO sample.

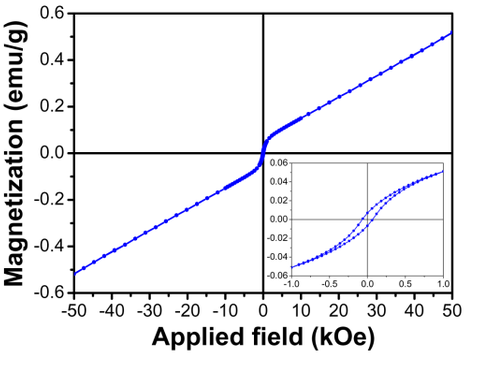

Figure 5. Magnetization of nanosized NiO calcined at 873 K in air as a function of field at 300 K measured by SQUID. The inset shows the low-field region of ± 1000 Oe.

ferromagnetism in the field range of ±1,000 Oe and outside this range the specific magnetization increases with increasing field. However, outside this range the specific magnetization increased with increasing field and showed no sign of saturation in the field range investigated (±50 kOe). The values of specific magnetization, 0.051 and 0.519 emu/g, were observed at 1,000 Oe and 50 kOe, respectively. The value of coercivity of 149 Oe is observed for NiO nanocrystalline powders calcined at 873 K (inset in Figure 5). These behaviors indicate that NiO nanocrystalline powders exhibit a ferromagnetic character in contrast to antiferromagnetic bulk material [33]. The appearance of the ferromagnetic-like behavior is probably due to the presence of superparamagnetic metallic Ni clusters or Ni^{3+} ions within the NiO lattice [13,34]. However, any traces of metallic Ni, Ni^{3+} ions and other ferromagnetic impurities were not detected by XRD and TEM. Therefore, the ferromagnetism in NiO nanocrystallites originates from the NiO nanocrystallite system.

Differentiation of the magnetization curve of the calcined NiO sample in Figure 5 with respect to the applied field yielded curves of mass susceptibility χ_m (emu/Oe.g), shown in Figure 6; outside of the hysteresis regions (-50,000 < H < -5,000 Oe and 5,000 < H < 50000 Oe), appeared to be constant. The mass susceptibility value of ~ 6×10^{-7} emu/Oe.g was observed in the NiO sample.

Although we have not determined the Ni charge state, it may be assumed that the Ni remains Ni (II) in our NiO sample, since we used Ni (II) complex as the Ni precursor. Considering this, with support from the XRD and SAED analysis results, the presence of sufficient Ni metal to explain the ferromagnetism at room temperature in our NiO nanocrystalline sample may be ruled out. The weak ferromagnetic-like behavior in our sample may be attributed to the broken bonds and lattice distortion [34-36]. It is well

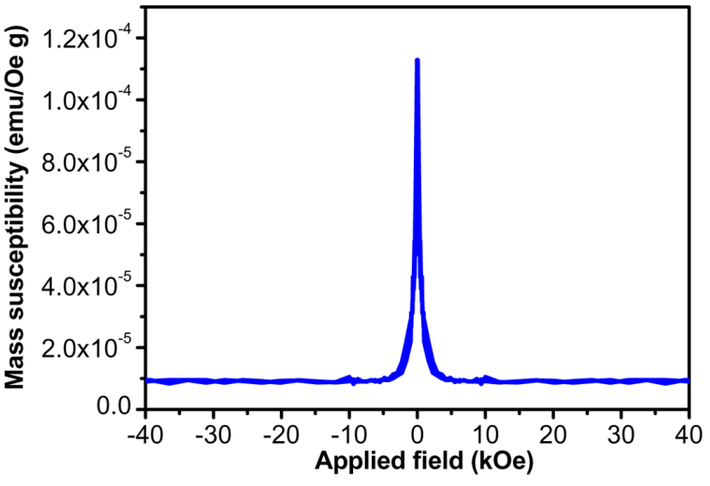

Figure 6. The mass susceptibility at 300 K obtained from differentiating the magnetization curves of nanosized NiO calcined at 873 K as a function of field.

known that the lattice distortion usually occurs in nanoscaled particles. The XRD result has also verified this phenomenon in the studied samples. For antiferromagnetic oxides, the superexchange interaction is sensitive to the local environment, such as the length and angle of bonds. The variation of lattice parameters should influence the strength of superexchange interaction, resulting in the appearance of weak ferromagnetism. It is believed that the ferromagnetic behavior is attributed to the combined effects of the lattice distortion and the broken bonds [11,34]. However, further work is needed to achieve a thorough understanding in the physical origin of ferromagnetism for nanoscaled antiferromagnetic particles.

4. CONCLUSION

Nanocrystalline NiO powders were successfully synthesized by the polymerized complex method using Ni nitrate, citric acid and ethylence glycol, and their structure, morphology and magnetic properties were investigated. The particle size of synthesized nanocrystalline powders is smaller than 55 nm, as estimated by TEM and the Williamson-Hall equation. The XRD pattern suggested the formation of cubic structure in the powders after calcination at 873 K, and electron diffraction studies also showed no evidence for the presence of minor phase of nickel metal. The FT-IR spectra indicated the formation of NiO. The synthesized powders exhibited UV absorption below 2.76 eV and the direct band gap was determined to be 3.06 eV. The nanocrystalline NiO powders showed ferromagnetic-like behavior with specific magnetizations of 0.051 emu/g at 1 kOe and 0.519 emu/g at 50 kOe. The origin of ferromagnetic-like behavior in the NiO nanocrystallites is due to the broken bonds combined with the lattice distortion.

ACKNOWLEDGMENT

The authors would like to thank the Department of Chemistry, Khon Kaen University for providing FT-IR facilities, Department of Material Science and Engineering, The University of Arizona, USA for providing TEM facilities, and the School of Physics, Trinity College (Dublin) for providing SQUID facilities. This work is supported by The Integrated Nanotechnology Research Center (INRC), Khon Kaen University, Thailand.

REFERENCES

[1] Abdul Khadar M., Biju V. and Inoue A., Effect of finite size on the magnetization behavior of nanostructured nickel oxide, *Mater. Res. Bull.*, 2003; **38**: 1341-1349.

[2] Morrish A.H. and Haneda K., Magnetic structure of small $NiFe_2O_4$ particles, *J. Appl. Phys.*, 1981; **52**: 2496-2498.

[3] Seehra M.S., Shim H., Dutta P. and Manivannan A., Interparticle interaction effects in the magnetic properties of NiO nanorods, *J. Appl. Phys.*, 2005; **97**: 10J509-3.

[4] Ibrahim M.M., Darwish S. and Seehra M., Nonlinear temperature variation of magnetic viscosity in nanoscale FeOOH particles, *Phys. Rev. B*, 1995; **51**: 2955-2959.

[5] Tejada J., Zhang X.X., Del Barco E., Hen□ndez J.M. and Chudnovsky M., Macroscopic resonant tunneling of magnetization in ferritin, *Phys. Rev. Lett.*, 1997; **79**: 1754-1757.

[6] Thota S. and Kumar J., Sol-gel and anomalous magnetic behaviour of NiO

nanoparticles, *J. Phys. Chem. Solids.*, 2007; **68**: 1951-1964.

[7] Bodker F., Hansen M.F., Bender Koch C. and Morup S., Particle interaction effects in antiferromagnetic NiO nanoparticles, *J. Magn. Magn. Mater.*, 2000; **221**: 32-36.

[8] Seehra M.S., Babu V. S., Manivannan A. and Lynn J.W., Neutron scattering and magnetic studies of ferrihydrite nanoparticles, *Phys. Rev. B*, 2000; **61**: 3513-3518.

[9] Ghosh M., Biswas K., Sundareshan A. and Rao C.N.R., MnO and NiO nanoparticles: synthesis and magnetic properties, *J. Mater. Chem.*, 2006; **16**: 106-111.

[10] Schuele W.J. and Deetscreek V.D., Appearance of a weak ferromagnetism in fine particles of antiferromagnetic materials, *J. Appl. Phys.*, 1962; **33**: 1136-1337.

[11] Kodama R.H., Makhlouf S.A. and Berkowitz A.E., Finite size effects in antiferromagnetic NiO nanoparticles, *Phys. Rev. Lett.*, 1997; **79**: 1393-1396.

[12] Kodama R.H. and Berkowitz A.E., Atomic-scale magnetic modeling of oxide nanoparticles, *Phys. Rev. B*, 1999; **59**: 6321-6336.

[13] Richardson J.T., Yiagas D.I., Turk B., Forster K. and Twigg M.V., Origin of superparamagnetism in nickel oxide, *J. Appl. Phys.*, 1991; 70: 6977-6982.

[14] Ichiyanagi Y., Wakabayashi N., Yamazaki J., Yamada S., Kimishima Y., Komatsu E. and Tajima H., Magnetic properties of NiO nanoparticles, *Physica B*, 2003; **329-333**: 862-863.

[15] Bi H., Li S., Zhang Y. and Du Y., Ferromagnetic-like behavior of utrafine NiO nanocrystallites, *J. Magn. Magn. Mater.*, 2004; **277**: 363-367.

[16] Pechini M.P., US Pat. No. 3, 330, 697 (1967).

[17] Wongsaprom K., Swatsitang E., Maensiri S., Srijaranai S. and Seraphin S., Room temperature ferromagnetism in Co-doped $La_{0.5}Sr_{0.5}TiO_{3-d}$, *Appl. Phys. Lett.*, 2007; **90**: 162506-3.

[18] Maensiri S., Wongsaprom K., Swatsitang E. and Seraphin S., Fe-doped $La_{0.5}Sr_{0.5}TiO_{3-d}$, *J. Appl. Phys.*, 2007; **102**: 076110-3.

[19] Maensiri S., Sreesongmuang J., Thomas C. and Klingkaewnarong J., Magnetic behavior of nanocrystalline powders of Co-doped ZnO diluted magnetic semiconductors synthesized by polymerizable precursor method, *J. Magn. Magn. Mater.*, 2006; **301**: 422-432.

[20] Klinkaewnarong J. and Maensiri S., Nanocrystalline hydroxyapatite powders by a polymerized complex method, *Chiang Mai J. Sci.*, 2010; **37**: 243-251.

[21] Cullity B.D., and Stock S.R., Elements of X-ray Diffraction, 3rd edn., Printice Hall, New Jersey, 2001.

[22] Zhou X.-D. and Huebner W., Size-induced lattice relaxation in CeO_2 nanoparticles, *Appl. Phys. Lett.*, 2001; **79**: 3512-3514.

[23] Qiao H., Wei Z., Yang H., Zhu L. and Yan X., Preparation and characterization of NiO nanoparticles by anodic arc plasma method, *J. Nanometer.*, 2009; **2009**: 1-5.

[24] Salavati-Niasari M., Mohandes F., Davar F., Mazaheri M., Monemzadeh M. and Yavarinia N., Preparation of NiO nanoparticles from metal-organic frameworks via a solid-state decom-

position route, *Inorg. Chim. Acta*, 2009; **362**: 3691-3697.

[25] Li H., Wang J., Liu H., Yang C., Xu H., Li X. and Cui H., Sol-gel preparation of transparent zinc oxide films with highly preferential crystal orientation, *Vacuum*, 2004; **77**: 57-62.

[26] Cheng X.L., Zhao H., Huo L.H., Gao S. and Zhao J.G., ZnO nanoparticulate thin film: Preparation, characterization and gas-sensing property, *Sens. Actuators B.*, 2004; **102**: 248-252.

[27] Kwon Y.J., Kim K.H., Lim C.S. and Shim K.B., Characterization of ZnO nanopowders synthesized by the polymerized complex method via organochemical route, *J. Ceram. Proc. Res.*, 2002; **3**: 146-149.

[28] Ziegler E., Heinrich A., Oppermann H. and Stover G., Electrical properties and non-stoichiometry in ZnO single crystals, *Phys. Status Solidi A*, 1981; **66**: 635-648.

[29] Uplane M.M., Mujawar S.H., Inamdar A.I., Shinde P.S., Sonavane A.C. and Patil P.S., Structural, optical and electrochomic properties of nickel oxide thin films grown from electrodeposited nickel sulphide, *Appl. Surf. Sci.*, 2007; **253**: 9365-9371.

[30] Granqvist C.G., Handbook of Inorganic Electrochromic Materials, Elsevier, Amsterdam, 1995.

[31] Al-Ghamdi A.A., Mahmoud W.E., Yagmour S.J. and Al-Marzouki F.M., Structure and optical properties of nanocrystalline NiO thin film synthesized by sol-gel spin-coating method, *J. Alloys Compd.*, 2009; **486**: 9-13.

[32] Maensiri S., Laokul P. and Promarak V., Synthesis and optical properties of nanocrystalline ZnO powders by a simple method using zinc acetate dehydrate, *J. Cryst. Growth*, 2006; **289**: 102-106.

[33] Chantrell R.W., El-Hilo M. and O'Grady K., Spin-glass behavior in a fine particle system, *IEEE Trans. Magn.*, 1991; **27**: 3570-3578.

[34] Bi H., Li S., Zhang Y. and Du Y., Ferromagnetic-like behavior of ultrafine NiO nanocrystallites, *J. Magn. Magn. Mater.*, 2004; **277**: 363-367.

[35] Makhlouf S.A., Parker F.T., Spada F.E. and Berkowitz A.E., Magnetic anomalies in NiO nanoparticles, *J. Appl. Phys.*, 1997; **81**: 5561-5563.

[36] Morrish A.H. and Haneda K., Magnetic structure of small $NiFe_2O_4$ particles, *J. Appl. Phys.*, 1981; **52**: 2496-2498.